High-throughput chromatin motion tracking in living yeast reveals the flexibility of the fiber throughout the genome

Houssam Hajjoul, Julien Mathon, Hubert Ranchon, Pascal Carrivain, Isabelle
Goiffon, Julien Mozziconacci, Benjamin Albert, Jean-Marc Victor, Olivier
Gadal, Kerstin Bystricky, et al.

HAL Id: hal-01053149
https://hal.science/hal-01053149

High throughput chromatin motion tracking in living yeast reveals the flexibility of the fiber throughout the genome

Houssam Hajjoul[1,3*], Julien Mathon[1,3*], Hubert Ranchon[1,3], Isabelle Goiffon[2,3], Julien Mozziconacci,[4,5] Benjamin Albert[2,3], Pascal Carrivain,[4,5] Jean-Marc Victor,[4,5] Olivier Gadal[2,3], Kerstin Bystricky[2,3], Aurélien Bancaud[1,3]

Keywords: chromatin / live cell imaging / high-throughput particle tracking / nuclear architecture / Brownian Dynamics Simulations

1: LAAS, CNRS, 7 avenue du colonel Roche, F-31400 Toulouse, France
2: LBME, CNRS, 118 route de Narbonne, F-31000 Toulouse, France
3: University of Toulouse, F-31062 Toulouse, France
4: LPTMC UMR 7600, CNRS, University Pierre et Marie Curie-Paris 6, 4 place Jussieu, 75252 Paris Cedex 05, France
5: CNRS GDR 3536, University Pierre et Marie Curie-Paris 6, 4 place Jussieu, 75252 Paris Cedex 05, France

[*] These authors participated equally to this work.

Corresponding author:

Aurélien Bancaud
email: abancaud@laas.fr
Phone: +33 (0)5 61 33 62 46; Fax: +33 (0)5 61 33 62 08;

ABSTRACT (211 words)

Chromosome dynamics are recognized to be intimately linked to genomic transactions, yet the physical principles governing spatial fluctuations of chromatin is still a matter of debate. Using high-throughput single particle tracking we record the movements of 9 fluorescently labeled chromosome loci located on chromosomes III, IV, XII, and XIV of *S. cerevisiae* over an extended temporal range spanning more than 4 orders of magnitude (10^{-2} to 10^{3} s). Spatial fluctuations appear to be characterized by an anomalous diffusive behavior, which is homogeneous in the time domain, for all sites analyzed. We show that this response is consistent with the Rouse polymer model, and we confirm the relevance of the model with Brownian dynamics simulations and the analysis of the statistical properties of the trajectories. Moreover the analysis of the amplitude of fluctuations by the Rouse model shows that yeast chromatin is highly flexible, its persistence length being qualitatively estimated to less than 30 nm. Finally we show that the Rouse model is also relevant to analyze chromosome motion in mutant cells depleted of proteins that bind to or assemble chromatin, and suggest that it provides a consistent framework to study chromatin dynamics. We discuss the implications of our findings for yeast genome architecture and for target search mechanisms in the nucleus.

INTRODUCTION

Chromosome higher order architecture has been increasingly studied over the last decade thanks to technological breakthroughs in imaging and in molecular biology ranging from painting single chromosomes in fixed cells (Cremer and Cremer 2001) to mapping physical interactions between genomic elements at the genome-wide level (Hi-C) (Dekker 2008). It is now established that chromosome large scale organization plays important roles in all aspects of genomic transactions, allowing contact between distant chromatin loci (Göndör and Ohlsson 2009) that trigger concomitant genomic processes in *cis* and in *trans*. Although several models have been proposed to describe the folding of chromosomes (Lieberman-Aiden et al. 2009; Bohn and Heermann 2010; Bancaud et al. 2012), the physical principles governing this organization are still largely debated.

Despite its small size, budding yeast has become a unique model that recapitulates some of the main features of higher eukaryotes, including heterochromatin-like regions, and an organization mediated by the nuclear envelope (NE), the nucleolus, and the spindle pole body (SPB). Structural data obtained by statistical positioning of a gene in a yeast cell population led to a surprisingly simple model to define yeast nuclear architecture (Zimmer and Fabre 2011): chromosome position can be predicted by few parameters such as genomic arm length, telomeres (TEL), and centromeres (CEN) tethered to the NE via nuclear-envelope-tethered proteins and to the SPB via microtubules, respectively (Bystricky et al. 2005; Therizols et al. 2010; Zimmer and Fabre 2011). This description was recently complemented by the first Hi-C comprehensive maps (Rodley et al. 2009; Duan et al. 2010), which confirmed an organization guided by nuclear landmarks, including TEL that congregate in foci (Gotta et al. 1996; Schober et al. 2008). Recent Brownian dynamics (BD) simulations confirmed this structural model by recapitulating Hi-C and imaging data,

assuming that physical tethering at TEL and CEN and volume exclusion were driving chromosome conformations (Tjong et al. 2012; Wong et al. 2012).

The large spatial fluctuations of chromosome loci inferred from particle tracking in living yeast suggested a highly dynamic character of chromosome architecture at the molecular level (Marshall et al. 1997; Heun et al. 2001; Hihara et al. 2012). Chromatin dynamics appeared to be determined by nuclear constraints, in particular the NE (Heun et al. 2001; Bystricky et al. 2004), and by the position along the chromosome, e.g. TEL (Bystricky et al. 2005). Furthermore, a large body of data provides information on spatio-temporal dynamics in wild type *vs*. mutant cells (see e.g. (Bystricky et al. 2009)) and elucidates how chromatin properties are regulated by structural proteins. However the quantitative analysis of these movements remains controversial, and essentially two models have been used: (i) chromatin segments were suggested to undergo normal Brownian fluctuations at small time scales, and to be confined in regions of ~0.3 μm^2 at time scales longer than ~100 s (Marshall et al. 1997); or (ii) the movement of GAL genes on chromosome II appeared to follow an anomalous behavior characterized by a diffusion coefficient of ~0.4 (Cabal et al. 2006). This anomalous behavior was also detected in bacteria (Weber et al. 2010) and thoroughly studied using polymer models. In yeast the narrow temporal range of measurements within less than two decades were insufficient for a truly quantitative analysis of chromatin dynamics.

Here we develop high-speed live cell imaging and high-throughput image analysis techniques to monitor the spatio-temporal fluctuations over an extended temporal range spanning more than 4 decades (10^{-2} to 10^3 s) of 9 chromosome loci on chromosomes III, IV, XII, and XIV of the yeast *S. cerevisiae*. We show that chromatin segments move sub-diffusively, and that the characteristics of the anomalous response are largely conserved for every locus distant by more than ~50 kb from TEL and CEN. Similar dynamic behavior was also observed for two telomeric loci whenever they adopt a central localization in the nucleus,

thus leading to a consistent picture for chromosome movement within the entire nuclear volume. We then demonstrate that these dynamics are consistent with the Rouse model using BD simulations and statistical analysis of the trajectories, and suggest that chromatin is a flexible polymer in yeast, characterized by a persistence length of less than 30 nm. Finally we show that the Rouse model is also relevant in mutants for proteins involved in chromatin structure, and propose that this model defines a consistent framework to study chromosome motion. Our findings significantly advance the quantitative understanding of chromosome dynamics and their implications for yeast genome architecture.

RESULTS AND DISCUSSION

The dynamics of chromosome loci are uniform throughout the nucleus and anomalous over a broad temporal range

We assayed the dynamics of chromatin in a collection of yeast strains each bearing a single fluorescently-labeled chromatin locus (see methods for details). The labels were inserted on chromosomes III, IV, XII, and XIV at loci distant from TEL and CEN (Fig. 1 and Fig. 2A). The chromosomes tested ranged in size from 300 kb to 1500 kb, which is well-suited to assess whether the dynamics are affected by chromosome length. Motion was analyzed over a temporal range spanning more than four decades (15 ms to 400 s, Fig. 2B). This broad temporal analysis is more than 2 orders of magnitude larger than in previous studies performed in living yeast (Heun et al. 2001; Bystricky et al. 2004; Cabal et al. 2006) or in bacteria (Weber et al. 2010), and investigations on similar time domains were only conducted in mammalian cells for telomere dynamics (Bronstein et al. 2009). The motion of chromosome loci was recorded using a bright field microscope, and analyzed using a

customized high-throughput tracking software based on the Multiple-Target Tracing algorithm ((Sergé et al. 2008); J.M. and A.B. in preparation and Supplementary Fig. S1). Because physical tethering of chromosomes may occur at the nuclear periphery (Heun et al. 2001; Hediger et al. 2002), the nucleus was divided into two regions of equal surfaces, and every tracked locus was automatically assigned to a central or peripheral localization based on the segmentation of the first image of the acquisitions (see image in Fig. 1).

We first focused on loci located in the nuclear center, far from constraints imposed by the nuclear membrane, and representing ~60 % of the observed positions (Fig. 2A). We then characterized their motion by plotting the temporal evolution of the mean square displacement (MSD), which describes the average displacement after a given time lag τ:

$$MSD(\tau) = \langle (\vec{r}(t + \tau) - \vec{r}(t))^2 \rangle \qquad (1)$$

with $\vec{r}$ the position vector, and $\langle - \rangle$ denoting the temporal average. We observed similar responses for every locus (data points in Fig. 2B), which appeared to fold onto a single master curve (solid line). This curve follows an anomalous diffusive behavior over a broad temporal range characterized by a power-law scaling response in t^{α} with α=0.52+/-0.08 (α=1 for normal diffusion). This result is consistant with an earlier study describing the motion of GAL genes, which exhibited a non linear MSD response characterized by an exponent of ~0.4 in the temporal range of 4 to 80 s (Cabal et al. 2006), but it departs from other contributions showing normal diffusion and a plateau in the long time limit (see e.g. (Heun et al. 2001)). The anomalous sub-diffusion response is associated with a slow increase in MSD over time. Its persistence an extended period indicates that chromatin loci explore a broad region of the nucleus of $\sqrt{0.2 \ \mu m^2}$~450 nm in ~400 s. This estimate is consistent with the extent of "gene territories" of ~500 nm, which are obtained by statistical mapping of the position of loci in cell populations of ~2000 individuals (Berger et al. 2008).

Next we studied the motion of chromosome loci located at the periphery, and observed that they frequently oscillated between nuclear center and periphery during the time course of the acquisition (Supplementary Fig. S1), suggesting that the localization classification based on a single image is somewhat artificial. We did not detect significant differences in the MSD response for peripheral or central localization for the three loci on chromosome XII (see e.g. position 240 kp in Fig. 2C) and on chromosome IV and XIV (not shown), so the anomalous diffusive response appears to be largely conserved and appropriate to describe chromosome segmental dynamics for loci distant by more than ~50 kb from TEL and CEN.

The dynamics of telomeres are anomalous in a central localization

In yeast, the 32 TEL tend to cluster near the NE, and the motion of tagged chromosome sites in the vicinity of a TEL is constrained (Heun et al. 2001; Sage et al. 2005). Using our reference behavior for chromosome loci located halfway along chromosome arms, we set out to perform an MSD analysis on TEL 3R and 14L (Fig. 1; hereafter denoted Tel3R and Tel14L). Though TEL predominantly accumulate near the periphery (Fig. 3A, right panel), their positioning in the nuclear center can be detected with an occurrence of ~30%, and we analyzed their dynamics in this central region. The amplitude of spatial fluctuations in the short time regime appeared to be relatively similar compared to the reference response (Fig. 3A), although Tel3R appeared to be slightly less mobile after ~10 s than Tel14L, presumably because telomeric interactions between the two ends of chromosome XIV are much less frequent than that of chromosome III (Bystricky et al. 2005; Duan et al. 2010).

In contrast to the bulk of chromosomes, telomere dynamics appeared to be reduced at the nuclear periphery (Fig. 3B), in agreement with the idea that telomere peripheral localization is mediated by protein interactions involving among others *SIR4* and

YKU70/YKU80 (Hediger et al. 2002; Taddei et al. 2004; Bupp et al. 2007; Schober et al. 2009). It has been shown that deletion of either *YKU70* or *SIR4* leads to delocalization of some TEL to the nuclear center (Laroche et al. 1998; Hediger et al. 2002), but it remains unclear whether this deletion affects TEL dynamics aside from chromosome III (Bystricky et al. 2009). We thus investigated the movements of Tel14L in wild-type and in *SIR4* mutant strains. Deletion of *SIR4* leads to a predominant localization of Tel14L in the center (62%), likely due to loss of anchoring to the nuclear membrane. Moreover telomere mobility is increased in *SIR4* mutant strains when the tagged locus resides at the periphery and even more drastically at the nuclear center (Fig. 3B), confirming that physical interactions of the extremities of chromosomes are an essential player of their spatio-temporal dynamics. Overall this study tends to support the proposition of uniform fluctuations throughout the nucleus for chromatin loci provided that they are sufficiently distant from anchoring regions.

Chromosome segmental dynamics are consistent with the Rouse model

To interpret our results with a polymer model, we make the assumptions that chromosome conformation and dynamics are mainly determined by (i) the permanent tethering of CEN to the SPB and the more transient attachment of TEL to NE (Zimmer and Fabre 2011), and (ii) the level of crowding mediated by chromosomes and nuclear proteins. Crowding is expected to screen out hydrodynamic effects, which otherwise induce long range interactions in between chromosome segments (Doi and Edwards 1988), so that nearest-neighbor elastic interactions between consecutive chromosome segments dominate their local dynamics. This approximation, which leads to the "Rouse" regime (Rouse 1953), has been extensively documented for concentrated solutions of synthetic polymers (see e.g. (Ewen and

Richter 1997)), and was recently validated *in vivo* for the bacterial chromosome (Weber et al. 2010).

Chromosomes are modeled by a Rouse chain, which is composed of a series of *N* elastic segments of length *b*. The motion of each bond is determined by its elasticity defined by the stiffness *$3k_BT/b^2$* with k_BT the thermal energy, and its viscous drag ζ. Assuming that chromosomes are tethered at CEN and TEL, the MSD of monomers can be solved analytically in the short time regime (see Model section):

$$MSD(\tau) \sim \left[\frac{12b^2 k_B T}{\pi \zeta}\right]^{1/2} \tau^{1/2} \qquad (2)$$

The Rouse segmental dynamics are characterized by an anomalous diffusive response uniform along the chain, in good agreement with our data. We wished to test the predictions of the Rouse model further by extracting the histogram of the displacement after a time lag of 0.18, 1.0 and 1.6 s from the trajectories of locus 240 on chromosome XII (Fig. 4A). The histograms were first fitted with a normal diffusion model (Fig. 4A, left panel and equation in inset), which relies on one fitting parameter, the diffusion coefficient *D*. The diffusion coefficient of 4.8, 2.2, 1.8 10^{-3} µm^2/s was very different for τ=0.18, 1.0, and 1.6 s, respectively, showing the inconsistency of this model. We then used the formalism described in (Guérin et al. 2012) to compute the histogram of the displacement for a Rouse chain tethered at its extremities (see expression in Model section). One single parameter was sufficient to reproduce the three distributions (Fig. 4A, right panel), and the quality of the fitting was significantly improved (note the departure of the red fit from the conventional model), hence strongly supporting the relevance of the Rouse model to describe the segmental dynamics of yeast chromosomes.

We then performed BD simulations of yeast chromosome dynamics in a volume the geometry of which is consistent with yeast nuclear size, and using the structure derived from Hi-C experiments as the initial state (Duan et al. 2010). We assumed that chromosomes were attached to the SPB at their CEN (*i.e.*, neglecting the contribution of microtubules connecting SPB to kinetochores), and freely diffusing at their TEL (chromosome III is represented in the left panel of Fig. 5B). The computed MSD for loci distant from CEN (>400 nm; blue dataset in the right panel of Fig. 5B) reproduced our the anomalous diffusive response associated to a power-law scaling of ~0.54 over a temporal domain of four orders of magnitude that we observed experimentally (dashed line in Fig. 5B, right panel). The motion is more restricted for segments located at 10-100 nm from the CEN (pink dataset) *vs*. at a distance comprised between 200-400 nm (red dataset). In addition, superposing the conformations of chromosome III during 10^6 time steps shows an elongated state of diameter ~300 nm. This conformation is associated with volume exclusion between chromosomes (see also Supplementary Fig. S4B), an effect that was recently shown to be a key parameter of yeast nuclear architecture (Tjong et al. 2012). We thus conclude that the dynamics of chromosome loci in living yeast are accurately described by the Rouse model.

The Rouse dynamics imply that chromosome segments search for target sites by compact exploration (de Gennes 1982), meaning that they systematically visit neighboring sites as they look for targets during repair or transcription activation (Condamin et al. 2007). Because the probability that chromosome loci find a nearby target is increased (Guigas and Weiss 2008), the Rouse dynamics are likely efficient to create specific chromosome contacts in *cis* or in *trans* over distances of less than ~400 nm, which are explored in a few minutes (Fig. 2B). The notion of territoriality remains controversial, whether it is absent based on the observation that broken ends of chromosomes are free to search the entire genome for appropriate partners (Haber and Leung 1996), or partial as telomere colocalisation and

coordinated movement would indicate (Bystricky et al. 2005). Future BD simulation studies should therefore evaluate whether and how compact exploration is related to chromosome territoriality in the yeast genome.

MSD fluctuations suggest that chromatin is highly flexible

The level of flexibility of a chromatin fiber is a matter of debate. *In vitro* single molecule experiments have shown that the persistence length l_p of nucleosome arrays is 20-30 nm (Cui and Bustamante 2000; Bancaud et al. 2006; Celedon et al. 2009; Kruithof et al. 2009). Conversely, analyses based on polymer models of in vivo distance measurements or Hi-C experiments (Bystricky et al. 2004; Dekker 2008; Tjong et al. 2012) provided estimates of ~200 nm and 66-134 nm, respectively. Physical modeling of the mechanical properties nucleosome arrays predicts a persistence length smaller than 30 nm for chromatin (Ben-Haïm et al. 2001; Schiessel et al. 2001), except in the case of highly ordered arrays with strong nucleosome-nucleosome interactions (Wedemann and Langowski 2002), in which case l_p increases to ~250 nm.

The amplitude of spatial fluctuations can be qualitatively linked to the flexibility of chromatin using the Rouse model, given that the bond length b and the viscous drag coefficient ζ are equal to $2l_p$ and $6\pi\eta l_p$ with η the viscosity, respectively (de Gennes 1979). Injecting this term in Eq. (2) implies that the amplitude of the MSD increases with the square root of the polymer persistence length. The extent of spatio-temporal fluctuations therefore increases as the rigidity of the fiber increases, in qualitative opposition to free diffusion of an isolated tracer that increases as the diameter of the particle decreases. The MSD response can then be predicted for a persistence length comprised between 50 and 200 nm, given that the nuclear viscosity is η~7+/-3 10^{-2} P based on GFP diffusion coefficient measurements (Kawai-

Noma et al. 2006; Slaughter et al. 2007). This conjecture exceeds our measurements by a factor of 10 to 20 (dashed lines in Fig. 5A). In contrast, fitting of our data with the Rouse model leads to an amplitude of the MSD of $1.0 +/-0.2 \ 10^{-2} \ \mu m^2/s^{-1/2}$ (solid line in Fig. 5A), suggesting that the persistence length of chromatin in living yeast is ~5 nm. <mark>This length scale is coherent with the dimensions of a single nucleosome, which is a ~5 nm by ~10 nm disk-like structure.</mark> Hence the analysis of chromosome motion suggests that chromatin is a flexible polymer *in vivo*.

Because the Rouse model is a simplified model that does not take volume exclusion between monomers into account, we wished to strengthen our conclusions by running BD of a single chain composed of self-avoiding segments (see model section). The extracted MSD shows an anomalous diffusive response, as well as the dependence on the persistence length and the viscous drag (Eq. (2)) expected from the Rouse model (Fig. 5B). This analysis showed that the numerical prefactor of Eq. (2) is underestimated by 1.4, suggesting that volume exclusion enhances the rate of spatial exploration. This difference implies that the persistence length of ~5 nm is overestimated, and a correct estimate may be as small as ~3 nm. This length scale, which is comparable to the DNA diameter, is unrealistic and <mark>points to an additional parameter related to the chromosomal environment.</mark>

Each MSD curve represented in Fig. 2B is the average response over a population of ~100 cells. The clonal variability of the spatio-temporal dynamics is not shown in this graph, although this variability is large, as inferred from the distribution of average displacements after a time lag of 0.1, 0.6, and 4.0 s for ~70 loci on chromosome XII (position 830, Fig. 5C). Because the difference between the average and the maximal or minimal MSD is about three-fold, this variability is unlikely related to changes in persistence length, which should vary over two orders of magnitude from 0.3 to 30 nm. We rather suggest that this variability is associated with the existence of dynamic chromosomal contacts, as previously indicated in

e.g. the dynamic random loop model derived to interpret distance measurements in human cells (Mateos-Langerak et al. 2009). Dynamic and random contacts should transiently restrict spatial exploration (Supplementary Fig. S5), reduce the effective diffusion of a genomic site over a population average, and hence lead to an apparent persistence length smaller than chromatin intrinsic properties. We propose that chromosome loci with maximal mean square displacements in the short time regime represent the "interaction-free" limit, because their motion is not hindered by distant contacts. Given that the difference between the average and the maximal MSD is less than three-fold (Fig. 5C), we can evaluate an upper limit for the persistence length of 3^2x3 nm <30 nm. Consequently, chromatin appears as a flexible polymer, and its persistence length can be qualitatively estimated to be less than ~30 nm.

Chromatin structural proteins alter chromosome mobility

Finally we investigated whether the dynamics of chromosomes was altered in the absence of chromatin structural proteins or chromatin assembly proteins. We first considered the HMG-like protein Spt2 in *S. cerevisiae,* which interacts with the histones H3 and H4 (Horn et al. 2002). The statics and the dynamics of one locus on chromosome XIV were assayed in WT and mutant *spt2* cells, showing an accumulation at the periphery for the mutant and similar MSD responses in the short time regime (Fig. 6, right and left panels, respectively). We then performed the same analysis with Hho1p (Levy et al. 2008), which is considered as the linker histone analog in *S. cerevisiae,* though its structure differs from linker histone in other organisms because it bears two globular domains. So far it remains unclear whether and how this protein participates in chromatin condensation. The deletion of *hho1* increases the proportion of spots detected in the nuclear center compared to wild type, and increases ~1.5-fold the amplitude of chromatin loci displacements (Fig. 6). Given that the

ratio Hho1p *vs*. nucleosome remains poorly estimated (comprised between 1:37 to 1:4 (Freidkin and Katcoff 2001; Downs et al. 2003)), these enhanced dynamics may be associated with the reduced frequency of chromosome interactions mediated by the two domains of Hho1 and/or with an onset in flexibility due to conformational changes at the nucleosome level. Finally, we probed the role of the nucleosome assembly chaperone Asf1, which is involved in replication-dependent and replication-independent chromatin assembly (Loyola and Almouzni 2004). As for *hho1*, the labeled locus appeared to be more frequently central than in wild type nuclei, and its mobility was 2.2-fold increased. The Rouse model therefore seems to account for the dynamics of chromosome loci in WT cells, as well as in *hho1, asf1 and spt2* mutants, suggesting that this approach is sufficiently generic to perform systematic motion analyses.

CONCLUSION

We demonstrate that the motion of chromosome loci in living yeast is characterized by anomalous sub-diffusion with an exponent of 0.52 over a temporal domain spanning more than 4 orders of magnitude. We then show that this response, which appears to be relevant for the analysis of WT and mutant cells, is consistent with the Rouse dynamics. Because the Rouse regime is characteristic of polymers in crowded environments, our result strengthens the relevance of polymer models for the description of the yeast genome (Gehlen et al. 2012; Tjong et al. 2012; Wong et al. 2012). In addition the Rouse dynamics is associated to compact exploration, implying that chromosome loci efficiently search for nearby targets. We speculate that this property guides chromosome interactions in *cis* and *trans*, and envision that this hypothesis can be tested using BD simulations in combination with Hi-C experiments aiming to evaluate the number of chromosome contacts as a function of the genomic distance.

Further the amplitude of chromatin spatio-temporal fluctuations shows that this polymer is flexible. Yet the cell-to-cell variability of the amplitude of chromosome movements only allows for a qualitative determination of the persistence length of less than 30 nm. We propose that this variability is associated to dynamic interactions between chromosomes, and future BD simulations may confirm or invalidate this conjecture, in turn providing new insights on the statics and the dynamics of the yeast genome.

The folding of interphase chromosomes in metazoans involves loops of variable sizes defining topological domains of 0.2 to 5 Mb (Nora et al. 2012; Sexton et al. 2012). Because the dimension of these domains, which can be described as end-tethered chromosome fragments, is consistent with the length of yeast chromosome arms, we speculate that the Rouse model is relevant to higher-order eukaryotes. This model has recently been implemented in numerical simulations (Bohn and Heermann 2010), showing that the dynamics of loop formation may interfere with the segmental motion of human chromosomes, an hypothesis that remains to be tested quantitatively *in vivo*.

MODEL

Dynamics

The motion of an end-tethered Rouse chain can be studied analytically using normal mode decomposition (Vandoolaeghe and Terentjev 2007), and the MSD of the nth-segment (MSD_n) reads:

$$MSD_n(\tau) = \frac{4Nb^2}{\pi^2} \sum_{p=1}^{\infty} \frac{1}{p^2} \left(1 - e^{-\tau/\tau_p}\right) sin^2 \left(\frac{p\pi n}{N}\right) \tag{3}$$

with τ_p the relaxation time of each mode $\tau_p = \tau_R/p^2$ and $\tau_R = L^2\zeta/3\pi^2 k_B T$ the Rouse time

identified as the longest relaxation time of the chain. Note that this equation is valid in 3D,

and its 2D version is readily obtained with a multiplication by 2/3 assuming that the motion is

isotropic. The temporal evolution of the MSD is plotted in Supplementary Fig. S4As). In the

short time limit ($\tau \ll \tau_R$), equation (3) is dominated by the terms with large p, and it can be

simplified to obtain Equation (2) given in the main text. In addition, the formalism described

in ((Guérin et al. 2012) ; see details in Supplementary Materials)   enables to extract the

distribution of the displacement R for the nth segment after a time lag τ:

$$P_n(R,\tau) = \frac{R}{\Psi_n(\tau)} exp - \left\{\frac{R^2}{2\Psi_n(\tau)}\right\} \tag{4}$$

$$\Psi_n(\tau) = \frac{2b^2}{N} \sum_{p=1}^{N} \sin^2\left(p\frac{n\pi}{N+1}\right) * \left\{\frac{1-\exp\left(-\frac{2\zeta b^2\tau}{k_B T}\left[1-\cos\left(p\frac{\pi}{N+1}\right)\right]\right)}{1-\cos\left(p\frac{\pi}{N+1}\right)}\right\} \tag{5}$$

The movements of chromosomes, which were modeled by a series of bead linked by

springs or ball-in-socket joints, was also analyzed by BD. The size of each bead was set to 15

nm in diameter, and it was assumed to contain ~3 nucleosomes, so that the full genome

consists of 27,000 beads. Chromosomes were constrained in a sphere of 2 µm in diameter,

and the CEN were fixed to the SPB using harmonic constraints. We used the Langevin

dynamics algorithm implemented in the NAMD software (Phillips et al. 2005) with an

appropriate in-house force field. The Langevin equation for the nth monomer has the form:

$$m_n \frac{d^2 x_n}{dt^2}(t) = -grad_{x_n}E + f_n(t) - m_n b_n \frac{dx_n}{dt}(t) \tag{7}$$

where the random force $f_n(t)$ is derived from a Gaussian distribution with the properties:

$$\langle f_n(t)\rangle = 0 \tag{8}$$

$$\langle f_n(t)f_n(0)\rangle = 2k_B T \zeta m_n \delta(t) \tag{9}$$

with ζ the friction coefficient. The energy E of each bead is the sum of three contributions associated to the confinement in the nucleus, the elasticity of the chain, and the repulsive interactions between monomers, which are expressed as:

$$E = E_{conf} + E_{spring} + E_{VdW} \tag{10}$$

$$E_{conf}(r < r_1) = 0 \text{ and } E_{conf}(r > r_1) = E_1(r - r_1)^4 \tag{11}$$

with r the distance of the bead to the center of the nucleus, and r_1 the radius of the nucleus.

$$E_{spring}(n, n+1) = k_s(r_n - r_{n+1})^2 \tag{12}$$

$$E_{VdW}(i,j) = U\left\{\left(\frac{R_{min}}{|r_i-r_j|}\right)^{12} - 2\left(\frac{R_{min}}{|r_i-r_j|}\right)^6\right\} \tag{13}$$

The parameters of this model can be found in Table 1. BD were run during 3.10^7 time steps, starting from the conformation obtained by Hi-C (Duan et al. 2010) equilibrated during 10^6 time steps. We also performed BD to investigate whether spatio-temporal fluctuations were different for 1, 4, or 10 segments, or for one segment of large diameter along the chain. We did not detect differences on the MSD response (not shown), in agreement with our observation of similar dynamics with Lac or Tet labeling, which measure ~10 and 7 kb in length, respectively.

MATERIALS AND METHODS

Plasmids and strains:

All the strains we used are described in the Supplemental table 1.

Cell culture

Cells were grown in YPD or YNB at 30°C starting from a fresh overnight culture. They were diluted at 10^6 cells/ml, and harvested when OD600 reached 4.10^6 cells/ml and rinsed twice with the corresponding SC media. Cells were then spread on a SC media patch containing 2% agarose and 2% glucose coated slide. A coverslip was deposited over the cells, and the construction was finally sealed with "VaLaP" (1/3 vaseline, 1/3 lanoline, 1/3 paraffin). Live microscopy was limited to 20 minutes after mounting the coverslip. Extreme care was taken to ensure that cells are at approximately equal stages of growth based on their shapes, as inferred from a single image of transmission light microscopy, and based on the nucleus shape using the roundness parameter *R* that was defined as:

$$R = 4\pi \times Surface/Perimeter^2 \qquad (14)$$

with *Surface* the number of pixels after segmentation of the nucleus, and *Perimeter* the outline in pixels (see Supplementary Fig. S2). We considered nuclei with *R>0.8* to avoid mitotic phenotypes.

Live cell imaging

Yeast cells were imaged at room temperature with a BX-51 upright microscope equipped with a laser diode (Lumencor), a 100X oil immersion objective (NA=1.4), and an EMCCD camera (Andor DU-897), as described in (Hajjoul et al. 2009). The excitation emission at 470+/-10 nm was set to 7.53 W/µm^2, about 100 times less than the value which is necessary for normal cells growth (Carlton et al. 2010), and we observed consecutive rounds of divisions during ~2 hours (not shown). For slow acquisitions of inter-frame intervals of 2 s or more, we used a 100X oil immersion objective with a variable NA set to ~1.1-1.2. The acquisition was performed with a shutter synchronized with the camera to minimize photobleaching, and we checked for drifts by monitoring the position of the center of the

nucleus in the first and last image of the recording. Optimal inter-frame intervals of ~20 ms were reached by cropping regions of interest, and using a 2*2 binning with the Andor iQ imaging software. The loss in pixel size resolution was compensated with a 2X lens placed in the microscope light path.

We focused on 2D single particle tracking, and checked that similar information were retrieved with 3D tracking using micro-mirrors ((Hajjoul et al. 2009; Hajjoul et al. 2011), Supplementary Fig. S3). We note that 2D acquisitions may bias MSD responses for loci preferentially localized at the periphery, because in some cases central loci in the projected view may be peripheral in the 3D nucleus.

Data analysis

Video sequences consisted in 300 consecutive images, and we displayed MSD traces on 150 time intervals at most in order insure the statistical relevance of mean displacements. The movement of chromosome loci were systematically analyzed using a custom software that was developed in Matlab (Mathworks, Natick, MA; (Sergé et al. 2008). This software, which will be described in detail elsewhere, enabled us to extract (*x*,*y*) coordinates by Gaussian fitting, to reconstruct the trajectories, and to compute the MSD and the step distribution function. Note that the MSD in fixed cells was 20- to 30-fold lower than in living cells (Supplementary Fig. S3B).

manuscript. We are grateful to Charlotte Galimow for strain construction and initial characterization of gene position.

Figure 1: *Collection of loci used to monitor chromosome spatio-temporal dynamics.* Arrows indicate the genomic positions at which TetO or LacO repeats were inserted in 4 chromosomes. These loci are also represented by orange spheres on the yeast nuclear map obtained by Hi-C (Duan et al. 2010). The two purple circles represent the telomers that were tracked with the same labeling technique, and the green circles correspond to the centromere. The preferred localization of these loci was scored using a subdivision of the nucleus into two regions of equal surface (orange and green for central and peripheral localizations, respectively).

Figure 2: *Chromatin dynamics in living budding yeast.* (A) The upper panel shows fluorescence micrographs of different yeast strains for inter-frame intervals of 200 ms (for inter-frame intervals of 16 – 50 ms and mutants; see supplementary Fig. S2), and the lower plot represents the spatial distribution of these loci in the nuclear volume. (B) The temporal evolution of the MSD for 7 different chromatin loci with central localization is plotted over a broad temporal range covering more than 4 orders of magnitude. This data shows a universal behavior characterized by an anomalous diffusive response associated to power low scaling comprised between $t^{0.44}$ and $t^{0.6}$ (thin dashed lines). The black solid line corresponds to the Rouse regime, which is associated to an exponent of 0.5 (see details in Fig. 4). Note that each dataset is the average over 30-200 trajectories, and that we selected tracks with signal to noise ratios (SNR) larger than 30 dB. (C) The MSD response for loci with central or peripheral localization is compared (yellow and green datasets, respectively), showing similar dynamics. The black solid line represents the behavior measured in (B). The departure of the two curves in the short time regime is associated to the lower SNR of peripheral loci (not shown).

Figure 3: *Telomere dynamics in living budding yeasts.* (A) The left plot represents the MSD temporal evolution for telomere XIV-L and III-R with central localization (red and blue datasets). The black solid line represents the average response obtained in Fig. 2B. The plot on the right shows that telomere preferentially accumulate at the periphery (green and orange bars, respectively). (B) The left plot represents the comparison of the MSD response for telomere XIV-L at a central or peripheral localization in wild type cells (open yellow and green symbols, respectively), or in *sir4* mutant strains (crossed symbols) favoring a central localization of telomere XIV-L.

Figure 4: *Rouse model for chromosome segmental dynamics.* (A) The two graphs represent the step distribution functions measured for three different time intervals, which are represented by dashed lines in Fig. 2A. The genomic position of the locus on chromosome XII is 240 kb, and the inter-frame interval of the acquisition is 59 ms. Note the deviation of the distributions toward longer displacements for increasing time lags, which is consistent with the progressive exploration of the nuclear volume. The three curves are fitted to a normal diffusion model (equation in the inset), or an end-tethered Rouse model (Eq. 4-5) (left and right panels, respectively). (B) Brownian dynamics simulation was implemented with polymer chains and in a realistic yeast nucleus using the nuclear conformation obtained by Hi-C as initial state (Duan et al. 2010). Chromosomes are tethered at their centromeres (green spheres) and free at their telomeres. The figure in the left panel represents the orthographic projection of 100 conformations of chromosome III in the course of one simulation of 10^6 time points. The polymer is elongated, and its diameter is ~300+/-50 nm. The MSD is computed for loci localized near the SPB, or at 200-400 nm and more than 400 nm from this anchor (purple, red, and blue datasets, respectively), showing that the response follows Rouse dynamics (black dashed line) provided that the locus is sufficiently distant from CEN.

Figure 5: *Assaying chromatin flexibility from MSD analysis.* (A) The MSD response plotted in Fig. 2B is represented in gray, and analyzed with the Rouse model for different values of the persistence length of 200, 50, and 5 nm, as specified in the inset. The dynamics of chromosome loci are consistent with highly flexible of chromatin. (B) Brownian dynamics simulations of an isolated chain containing 100 segments have been performed to confirm the relevance of the Rouse model. Dimensionless variables are defined using l_p and $\eta l_p^3/k_B T$ as characteristic length and time scales, the MSD of a central monomer is plotted with different persistence lengths of 15, 30, 60, or 90 nm and for two different viscosities of 10^{-3} and 10^{-2} P (blue datasets). These datasets fall on a master curve, which follows the power law scaling of the analytical Rouse model: the black dashed line is derived from Equation (2) using the dimensionless variables (see exact expression in inset). (C) The histogram of the average square displacement after 0.1, 0.6, and 4.0 s is represented for ~70 loci on chromosome XII (position 680), with a broad cell to cell variability within a single clone. The lines are Gaussian fits and serve as guides to the eye.

Figure 6: *Chromatin structural/modifying proteins and chromosome dynamics.* The left plot represents the MSD temporal evolution for a locus on chromosome XIV, genomic position 240 kb. The wild type situation was identical to the Rouse response described in Fig. 3A, and it is represented by the black solid line. The dynamic response obtained in *hho1, asf1* and *spt2* utant yeast is represented by red, blue, and purple symbols, respectively. The two dashed lines represent fits to the data with the Rouse model. The plot in the right shows that *Asf1* and *Hho1* participate in the nuclear localization of the tagged locus (the yellow and green bars correspond to central and peripheral localizations, respectively).

T	300 K
k_s	1 kcal.mol^{-1}.nm^{-2}
R_{min}	7 nm
U	-0.01 kcal.mol^{-1}
m_n	10 a.u.
b_n	10 a.u.
E_1	0.01 kcal.mol^{-1}.nm^{-4}

Table 1: Set of parameters to run Brownian dynamics simulations.

REFERENCES

Bancaud A, Conde e Silva N, Barbi M, Wagner G, Allemand JF, Mozziconacci J, Lavelle C, Croquette V, Victor JM, Prunell A et al. 2006. Structural plasticity of single chromatin fibers revealed by torsional manipulation. *Nat Struct Mol Biol* **13**(5): 444-450.

Bancaud A, Lavelle C, Huet S, Ellenberg J. 2012. A fractal model for nuclear organization: current evidence and biological implications. *Nucl Acids Res* **40**: 8783-8792.

Ben-Haïm E, Lesne A, Victor JM. 2001. Chromatin: a tunable spring at work inside chromosomes. *Phys Rev E Stat Nonlin Soft Matter Phys* **64**: 051921.

Berger A, Cabal G, Fabre E, Duong T, Buc H, Nehrbass U, Olivo-Marin J, Gadal O, Zimmer C. 2008. High-resolution statistical mapping reveals gene territories in live yeast. *Nat Meth* **5**(12): 1031-1037.

Bohn M, Heermann DW. 2010. Diffusion-Driven Looping Provides a Consistent Framework for Chromatin Organization. *PLoS One* **5**: e12218.

Bronstein I, Israel Y, Kepten E, Mai S, Shav-Tal Y, Barkai E, Garini Y. 2009. Transient anomalous diffusion of telomeres in the nucleus of mammalian cells. *Phys Rev Lett* **103**(1): 18102.

Bupp JM, Martin AES, E. S., Jaspersen SL. 2007. Telomere anchoring at the nuclear periphery requires the budding yeast Sad1-UNC-84 domain protein Mps3. *JCB* **179**: 845-854.

Bystricky K, Heun P, Gehlen L, Langowski J, Gasser SM. 2004. Long range compaction and flexibility of interphase chromatin in budding yeast analysed by high-resolution imaging techniques. *Proc Natl Acad Sci U S A* **101**: 16495-16500.

Bystricky K, Laroche T, Van Houwe G, Blaszczyk M, Gasser S. 2005. Chromosome looping in yeast. *JCB* **168**(3): 375.

Bystricky K, Van Attikum H, Montiel M, Dion V, Gehlen L, Gasser S. 2009. Regulation of nuclear positioning and dynamics of the silent mating type loci by the yeast Ku70/Ku80 complex. *Mol Cell Biol* **29**(3): 835.

Cabal G, Genovesio A, Rodriguez-Navarro S, Zimmer C, Gadal O, Lesne A, Buc H, Feuerbach-Fournier F, Olivo-Marin J, Hurt E. 2006. SAGA interacting factors confine sub-diffusion of transcribed genes to the nuclear envelope. *Nature* **441**(7094): 770-773.

Carlton P, Boulanger J, Kervrann C, Sibarita J, Salamero J, Gordon-Messer S, Bressan D, Haber J, Haase S, Shao L. 2010. Fast live simultaneous multiwavelength four-dimensional optical microscopy. *Proc Nat Acad Sci USA* **107**(37): 16016.

Celedon A, Nodelman IM, Wildt B, Dewan R, Searson P, Wirtz D, Bowman GD, Sun SX. 2009. Magnetic tweezers measurement of single molecule torque. *Nano Lett* **9**: 1720-1725.

Condamin S, Bénichou O, Tejedor V, Voituriez R, Klafter J. 2007. First-passage times in complex scale-invariant media. *Nature* **450**: 77-80.

Cremer T, Cremer C. 2001. Chromosome territories, nuclear architecture and gene regulation in mammalian cells. *Nat Rev Genet* **2**: 292-301.

Cui Y, Bustamante C. 2000. Pulling a single chromatin fiber reveals the forces that maintain its higher-order structure. *Proc Natl Acad Sci U S A* **97**: 127-132.

de Gennes P-G. 1979. *Scaling concepts in polymer physics*. Cornell university press, Ithaca.

de Gennes PG. 1982. Kinetics of diffusion-controlled processes in dense polymer systems. I. Nonentangled regimes. *J Chem Phys* **76**: 3316-3321.

Dekker J. 2008. Mapping in vivo Chromatin interactions in yeast suggests an extended chromatin fiber with regional in compaction. *J Biol Chem* **283**: 34532.

Doi M, Edwards S. 1988. *The theory of polymer dynamics*. Oxford University Press, USA.

Downs JA, Kosmidou E, Morgan A, Jackson SP. 2003. Suppression of Homologous Recombination by the Saccharomyces cerevisiae Linker Histone. *Mol Cell* **11**(6): 1685-1692.

Duan Z, Andronescu M, Schutz K, McIlwain S, Kim YJ, Lee C, Shendure J, Fields S, Blau CA, Noble WS. 2010. A three-dimensional model of the yeast genome. *Nature* **465**(7296): 363-367.

Ewen B, Richter D. 1997. Neutron Spin Echo Investigations on the Segmental Dynamics of Polymers in Melts, Networks and Solutions. In *Advances in Polymer Science*, Vol 134, pp. 1-129. Springer Berlin / Heidelberg.

Freidkin I, Katcoff DJ. 2001. Specific distribution of the Saccharomyces cerevisiae linker histone homolog HHO1p in the chromatin. *Nucl Acids Res* **29**(19): 4043-4051.

Gehlen LR, Gruenert GM, Jones B, Rodley CD, Langowski J, O'Sullivan JM. 2012. Chromosome positioning and the clustering of functionally related loci in yeast is driven by chromosomal interactions. *Nucleus* **3**: 370 - 383.

Göndör A, Ohlsson R. 2009. Chromosome crosstalk in three dimensions. *Nature* **461**: 212-217.

Gotta M, Laroche T, Formenton A, Maillet L, Scherthan H, Gasser S. 1996. The clustering of telomeres and colocalization with Rap1, Sir3, and Sir4 proteins in wild-type Saccharomyces cerevisiae. *JCB* **134**(6): 1349-1363.

Guérin T, Bénichou O, Voituriez R. 2012. Non-Markovian polymer reaction kinetics. *Nat Chem* **4**: 568-573.

Guigas G, Weiss M. 2008. Sampling the cell with anomalous diffusion - the discovery of slowness. *Biophys J* **94**: 90-94.

Haber JE, Leung W-Y. 1996. Lack of chromosome territoriality in yeast: Promiscuous rejoining of broken chromosome ends *Proc Natl Acad Sci U S A* **93**: 13949-13954.

Hajjoul H, Kocanova S, Lassadi I, Bystricky K, Bancaud A. 2009. Lab-on-Chip for fast 3D particle tracking in living cells. *Lab on a Chip* **9**: 3054-3058.

Hajjoul H, Mathon J, Viero Y, Bancaud A. 2011. Optimized micromirrors for Three-dimensional single-particle tracking in living cells. *App Phys Lett* **98**: 243701.

Hediger F, Neumann F, Van Houwe G, Dubrana K, Gasser S. 2002. Live Imaging of Telomeres:: yKu and Sir Proteins Define Redundant Telomere-Anchoring Pathways in Yeast. *Curr Biol* **12**(24): 2076-2089.

Heun P, Laroche T, Shimada K, Furrer P, Gasser S. 2001. Chromosome dynamics in the yeast interphase nucleus. *Science* **294**(5549): 2181.

Hihara S, Pack C-G, Kaizu K, Tani T, Hanafusa T, Nozaki T, Takemoto S, Yoshimi T, Yokota H, Imamoto N et al. 2012. Local Nucleosome Dynamics Facilitate Chromatin Accessibility in Living Mammalian Cells. *Cell Reports* **2**(6): 1645-1656.

Horn PJ, Crowley KA, Carruthers LM, Hansen JC, Peterson CL. 2002. The SIN domain of the histone octamer is essential for intramolecular folding of nucleosomal arrays. *Nat Struct Biol* **9**: 167-171

Kawai-Noma S, Ayano S, Pack C-G, Kinjo M, Yoshida M, Yasuda K, Taguchi H. 2006. Dynamics of yeast prion aggregates in single living cells. *Genes to Cells* **11**(9): 1085-1096.

Kruithof M, Chien F-T, Routh A, Logie C, Rhodes D, van Noort J. 2009. Single-molecule force spectroscopy reveals a highly compliant helical folding for the 30 nm chromatin fiber. *Nat Struct Mol Biol* **16**: 534-540.

Laroche T, Martin SG, Gotta M, Gorham HC, Pryde FE, Louis EJ, Gasser SM. 1998. Mutation of yeast Ku genes disrupts the subnuclear organization of telomeres. *Curr Biol* **8**: 653-657.

Levy A, Eyal M, Hershkovits G, Salmon-Divon M, Klutstein M, Katcoff DJ. 2008. Yeast linker histone Hho1p is required for efficient RNA polymerase 1 processivity and transcriptional silencing at the ribosomal DNA. *Proc Natl Acad Sci U S A* **105**: 11703-11708.

Lieberman-Aiden E, van Berkum NL, Williams L, Imakaev M, Ragoczy T, Telling A, Amit I, Lajoie BR, Sabo PJ, Dorschner MO et al. 2009. Comprehensive Mapping of Long-Range Interactions reveals folding principles of the Human Chromosome. *Science* **326**: 289-293.

Loyola A, Almouzni G. 2004. Histone chaperones, a supporting role in the limelight. *Biochimica et Biophysica Acta* **1977**: 3-11.

Marshall W, Straight A, Marko J, Swedlow J, Dernburg A, Belmont A, Murray A, Agard D, Sedat J. 1997. Interphase chromosomes undergo constrained diffusional motion in living cells. *Current Biology* **7**(12): 930-939.

Mateos-Langerak J, Bohn M, de Leeuw W, Giromus O, Manders EM, Verschure PJ, Indemans MH, Gierman HJ, Heermann DW, van Driel R et al. 2009. Spatially confined folding of chromatin in the interphase nucleus. *Proc Natl Acad Sci U S A* **106**: 3812-3817.

Nora EP, Lajoie BR, Schulz EG, Giorgetti L, Okamoto I, Servant N, Piolot T, van Berkum NL, Meisig J, Sedat J et al. 2012. Spatial partitioning of the regulatory landscape of the X-inactivation centre. *Nature* **485**(7398): 381-385.

Phillips JC, Braun R, Wang W, Gumbart J, Tajkhorshid E, Villa E, Chipot C, Skeel RD, Kalé L, Schulten K. 2005. Scalable molecular dynamics with NAMD. *Journal of Computational Chemistry* **26**(16): 1781-1802.

Rodley CDM, Bertels F, Jones B, O'Sullivan JM. 2009. Global identification of yeast chromosome interactions using genome conformation capture. *Fungal Genetics and Biology* **46**: 879–886.

Rouse PE. 1953. A Theory of the Linear Viscoelastic Properties of Dilute Solutions of Coiling Polymers *J Chem Phys* **21**: 1272-1280.

Sage D, Neumann F, Hediger F, Gasser S, Unser M. 2005. Automatic tracking of individual fluorescence particles: application to the study of chromosome dynamics. *Image Processing, IEEE Transactions on* **14**(9): 1372-1383.

Schiessel H, Gelbart WM, Bruinsma R. 2001. DNA folding: structural and mechanical properties of the two-angle model for chromatin. *Biophys J* **80**: 1940-1956.

Schober H, Kalck V, Vega-Palas M, Van Houwe G, Sage D, Unser M, Gartenberg M, Gasser S. 2008. Controlled exchange of chromosomal arms reveals principles driving telomere interactions in yeast. *Genome research* **18**(2): 261.

Schober HF, H., Kalck V, Gehlen LR, Gasser SM. 2009. Yeast telomerase and the SUN domain protein Mps3 anchor telomers and repress subtelomeric recombination. *Genes & Dev* **23**: 928-938.

Sergé A, Bertaux N, Rigneault H, Marguet D. 2008. Dynamic multiple-target tracing to probe spatiotemporal cartography of cell membranes. *Nat Meth* **5**: 687-694.

Sexton T, Yaffe E, Kenigsberg E, Bantignies Fdr, Leblanc B, Hoichman M, Parrinello H, Tanay A, Cavalli G. 2012. Three-Dimensional Folding and Functional Organization Principles of the Drosophila Genome. *Cell* **148**(3): 458-472.

Slaughter BD, Schwartz JW, Rong L. 2007. Mapping dynamic protein interactions in MAP kinase signaling using live-cell fluorescence fluctuation spectroscopy and imaging. *Proc Natl Acad Sci U S A* **104**: 20320-20325.

Taddei A, Hediger F, Neumann FR, Bauer C, Gasser SM. 2004. Separation of silencing from perinuclear anchoring functions in yeast Ku80, Sir4 and Esc1 proteins. *EMBO J* **23**(6): 1301-1312.

Therizols P, Duong T, Dujon B, Zimmer C, Fabre E. 2010. Chromosome arm length and nuclear constraint determine the dynamic relationship of yeast subtelomeres. *Proc Natl Acad Sci USA* **107**: 2025-2030.

Tjong H, Gong K, Chen L, Alber F. 2012. Physical tethering and volume exclusion determine higher-order genome organization in budding yeast. *Genome Res* **22**(7): 1295-1305.

Vandoolaeghe WL, Terentjev EM. 2007. A Rouse-tube model of dynamic rubber viscoelasticity *J Phys A: Math Theor* **40**: 14725.

Weber S, Spakowitz A, Theriot J. 2010. Bacterial Chromosomal Loci Move Subdiffusively through a Viscoelastic Cytoplasm. *Phys Rev Lett* **104**(23): 238102.

Wedemann G, Langowski J. 2002. Computer simulation of the 30-nanometer chromatin fiber. *Biophys J* **82**: 2847-2859.

Wong H, Marie-Nelly H, Herbert SC, P., Blanc H, Koszul R, Fabre E, Zimmer C. 2012. A predictive computational model of the dynamic 3D interphase nucleus. *Curr Biol* **22**: 1881-1890.

Zimmer C, Fabre E. 2011. Principles of chromosomal organization: lessons from yeast. *JCB* **192**(5): 723-733.

High throughput chromatin motion tracking in living yeast reveals the flexibility of the fiber throughout the genome

Houssam Hajjoul[1,3*], Julien Mathon[1,3*], Hubert Ranchon[1,3], Isabelle Goiffon[2,3], Julien Mozziconacci,[4,5] Benjamin Albert[2,3], Pascal Carrivain,[4,5] Jean-Marc Victor,[4,5] Olivier Gadal[2,3], Kerstin Bystricky[2,3], Aurélien Bancaud[1,3]

Supplementary material contains: 1supplementary text, and 5 figures

Supplementary Material

  1- Model for step distribution analysis

We use the method developed by Guérin *et al.* to derive the step distribution function. We first define the Rouse modes for an end-tethered polymer chain, which requires to diagonalize the Hessian matrix. This matrix of size N^2 relates the elastic forces acting on each monomer, and it is tridiagonal:

$$\begin{pmatrix} 2 & -1 & 0 & \cdots & \cdots & \cdots \\ -1 & 2 & -1 & 0 & \cdots & \cdots \\ 0 & -1 & 2 & -1 & 0 & \cdots \\ \cdots & \cdots & \cdots & \cdots & \cdots & \cdots \\ \cdots & \cdots & \cdots & -1 & 2 & -1 \\ \cdots & \cdots & \cdots & 0 & -1 & 2 \end{pmatrix} \qquad (S1)$$

Note that this matrix is slightly different from that described in (Guérin et al. 2012) to account for the difference in boundary conditions. Its eigenvalues are:

$$\lambda_j = 2\left\{1 - cos\left(j\frac{\pi}{N+1}\right)\right\} \qquad (S2)$$

Its eigenvectors are:

$$Q_{ij} = \sqrt{\frac{2}{N}} \sin\left(ij\frac{\pi}{N+1}\right) \qquad (S3)$$

Using Supplementary Eq. A29-A30 of the work of Guérin *et al.*, we deduce the temporal evolution of a diffusive observable X:

$$\psi(t) = 2\sum_{j=1}^{N} \frac{b_j^2\left(1-e^{-\lambda_j t}\right)}{\lambda_j} \qquad (S4)$$

$$P(X,t) = \frac{1}{\sqrt{2\pi\psi}} e^{-\frac{X^2}{2\psi}} \qquad (S5)$$

In our case, we focus on the dynamics of a segment located at position n along the chromosome, and the terms b_j are defined by the following equations:

$$b_j = Q_{nj} = \sqrt{\frac{2}{N}} \sin\left(nj\frac{\pi}{N+1}\right) \qquad (S6)$$

These solutions are obtained with dimensionless variables, and we have to define the useful units of time and length:

$$\tau = \frac{\zeta b^2}{k_B T} \text{ and } l = b \qquad (S7)$$

Using the set of equations (S2,4,5,6,7), one can derive equation (5) and (6) given in the main text.

Supplementary Table 1: Strain list

Supplementary Figures

Figure S1: *High-throughput tracking and segmentation.* Starting from the raw data (upper left image), we automatically define whether the locus has a central or peripheral localization. For this the contour of the nucleus is extracted, and adjusted by a circle to evaluate its radius

(upper right image), and the distance of the locus to the nuclear center and to the edge of the nucleus is automatically measured. In the middle panel, the segmented nucleus and the locus trajectory are represented (left image), and the nuclear center is represented by a green outline (right image). In the bottom panel, we show the segmented nucleus as derived from our automatic software analysis (J.M., A.B. in preparation).

Figure S2: Fluorescence micrographs of the different yeast strains used for this study (inter-frame intervals are mentioned in the inset).

Figure S3: *Comparison of 2D vs. 3D particle tracking.* (A) We placed yeast cells tagged at position 194 kb on chromosome III on our microfabricated device for 3D microscopy based on tilted micromirrors (Hajjoul et al. 2009), and we monitored the movements of the locus in 2D and in 3D using one and two side views of the sample, respectively (see image in inset). MSD curves were fitted to the Rouse model, showing an expected difference of 2/3 in spatial fluctuations between the 2D and 3D response (see insets on the graph). (B) Comparison of MSD response in living and fixed yeast cells (blue and black datasets, respectively) in linear and logarithmic scales (right and left plots, respectively).

Figure S4: (A) *Analytical model of the segmental dynamics of an isolated end-tethered chain.* The left panel represents the temporal evolution of the MSD for a segment located half-, fifth-, or tenth-way through an end-tethered polymer (blue, green, and red curves, respectively). The plot in the right shows the MSD maximal amplitude vs. the genomic position of the locus (blue, green, and red data points are color-coded as in the left graph). Note that equation is consistent with this picture: when we consider the long time regime ($\tau \gg \tau_R$), the exponential term in equation (3) vanishes, and the discrete sum admits an analytical solution:
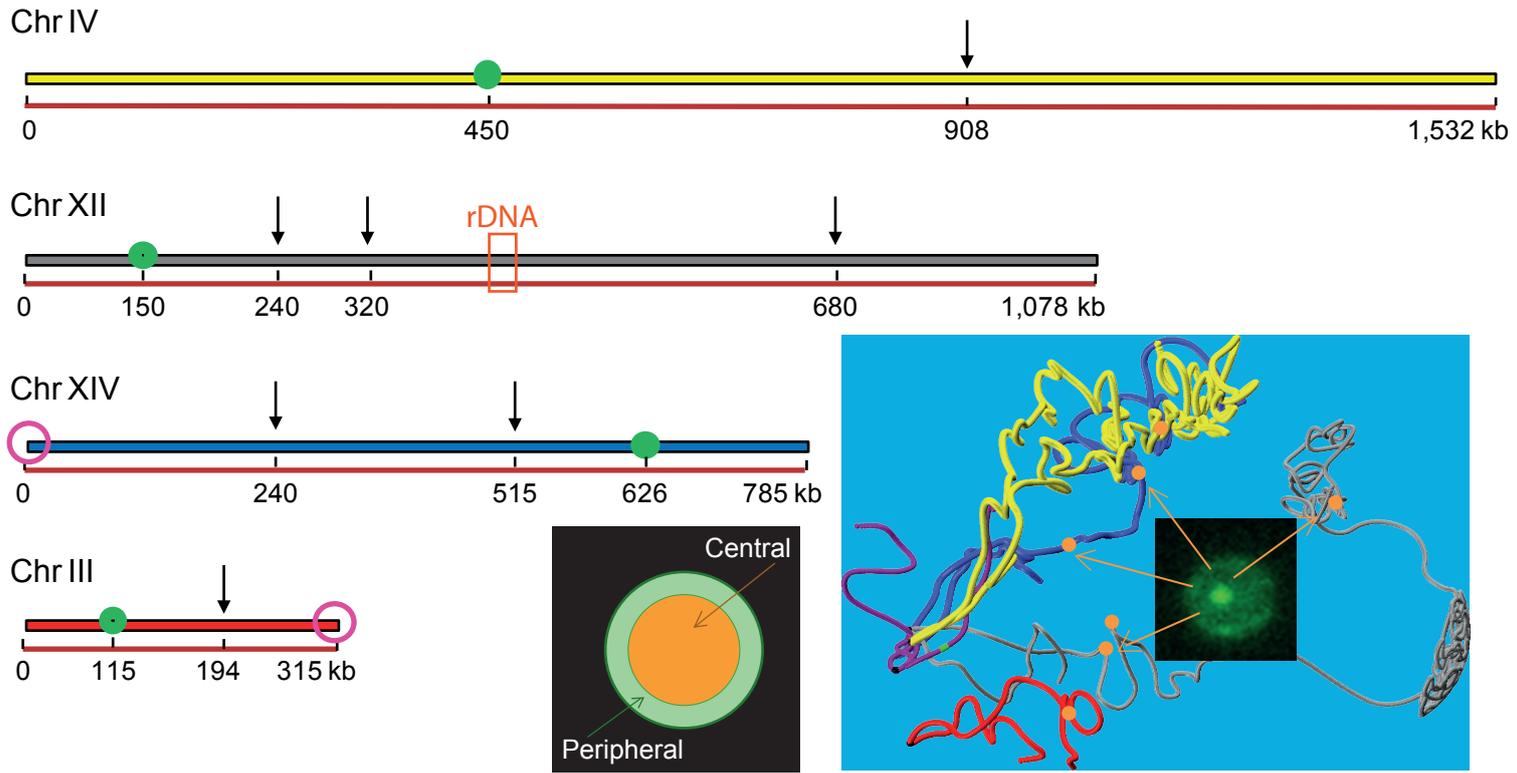
$$MSD_n(\tau \gg \tau_R) \sim 2Lb\left(\left(\frac{n}{N}\right)^2 - \frac{n}{N}\right) \tag{S8}$$

The amplitude of spatial fluctuations is thus greater for a monomer located halfway between the chain *vs*. close to the tethering ends, as expected from the folding of the polymer in an arch-shape.
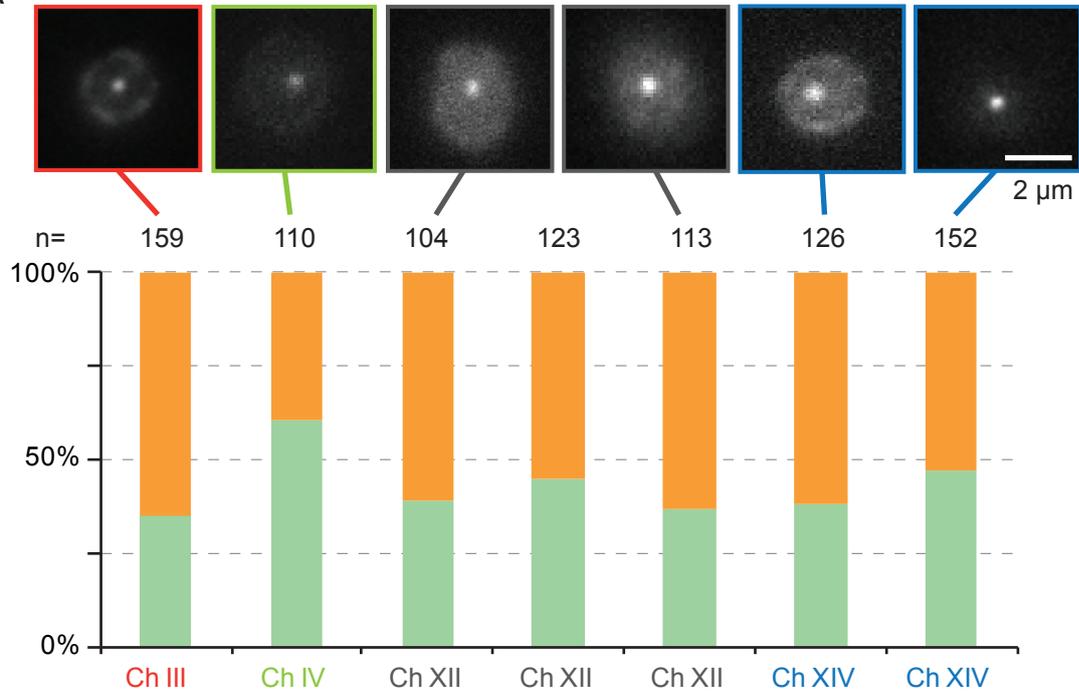
(B) *Visualization of the tube in molecular dynamics simulations.* The four images are snapshots representing the density of chromosome segments around chromosome III (continuous blue fiber). Segments of all other chromosomes, which are distant by less than 30, 50, 80, 150 nm (clockwise from upper left to lower left images, respectively), are color-coded using the same convention as in (Duan et al. 2010), illustrating the effect of volume exclusion between chromosomes.

Figure S5: *Chromosome contacts and slowed down MSD responses.* (A) Representation of a chromosome arm with two contacts that restrict the motion of one locus tagged in yellow. (B) The motion of the locus is dictated by the Rouse response in the small time regime, and anchors define a plateau of the MSD curve, which is dependent on the distance to the anchor, as described in Fig. S4A. The anchor is transient, and upon release, MSD increases to follow the Rouse model until reaching the next plateau determined by more distant contacts on the chromosome. (C) Dynamic and random contacts shift the average MSD response, plotted in logarithmic scale, along the temporal axis. Note that the response in the short time limit is representative of contact-free dynamics, because chromosome loci do not sense any restriction in motion.
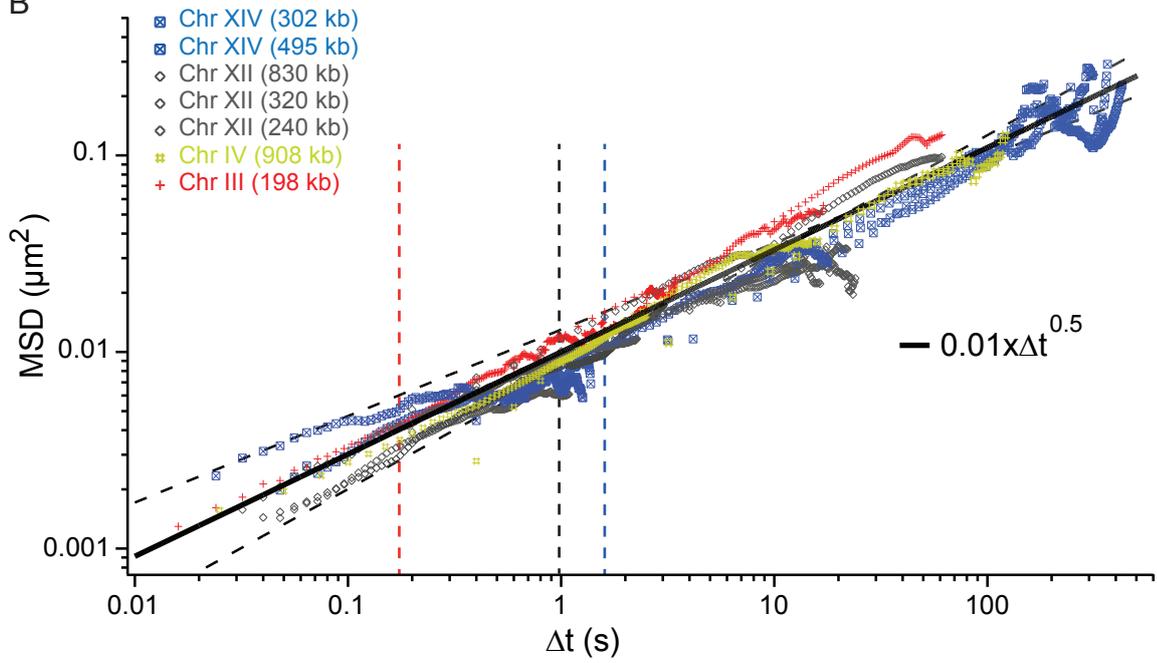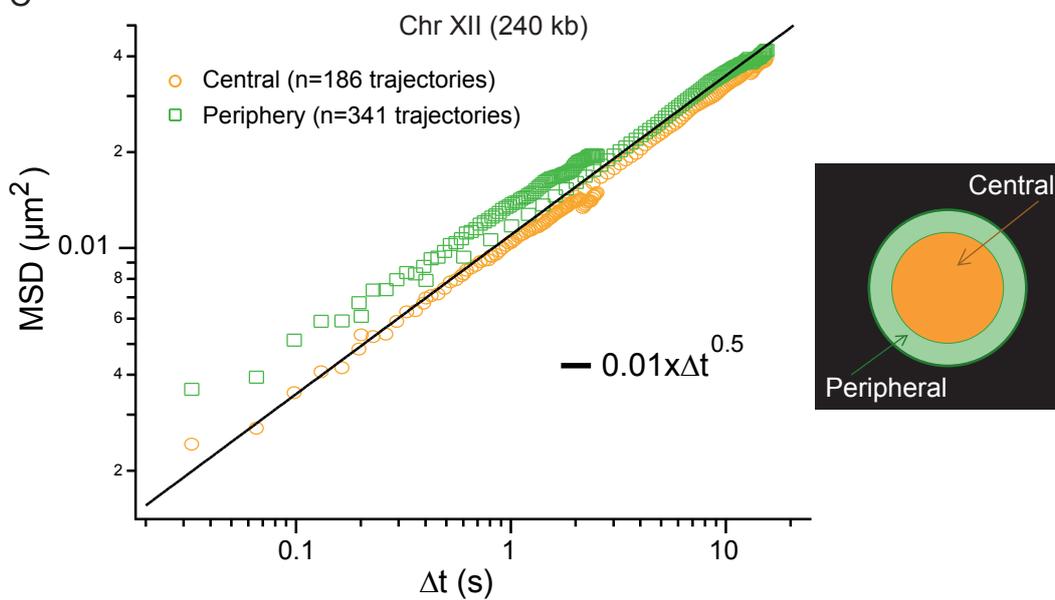
Figure 1

Hajjoul/Mathon *et al.*
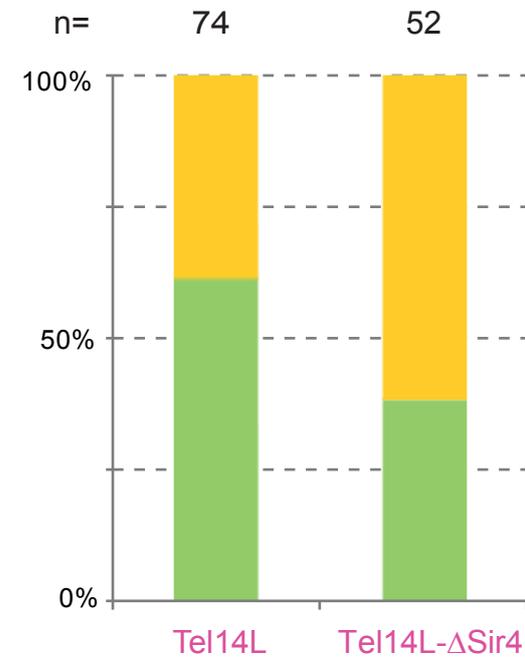
Chr IV

0   450   908   1,532 kb

Chr XII

rDNA

0   150   240   320   680   1,078 kb

Chr XIV

0   240   515   626   785 kb

Chr III

0   115   194   315 kb

Central

Peripheral

Figure 2   Hajjoul / Mathon et al.

A

n= 159 110 104 123 113 126 152

Ch III   Ch IV   Ch XII   Ch XII   Ch XII   Ch XIV   Ch XIV

B

- ⊠ Chr XIV (302 kb)
- ⊠ Chr XIV (495 kb)
- ◇ Chr XII (830 kb)
- ◇ Chr XII (320 kb)
- ◇ Chr XII (240 kb)
- ✳ Chr IV (908 kb)
- + Chr III (198 kb)

MSD (μm^2)

— $0.01 \times \Delta t^{0.5}$

Δt (s)

C

Chr XII (240 kb)

- ○ Central (n=186 trajectories)
- □ Periphery (n=341 trajectories)

MSD (μm^2)

— $0.01 \times \Delta t^{0.5}$

Central

Peripheral

Δt (s)

Figure 3   Hajjoul / Mathon et al.

Figure 4   Hajjoul/Mathon *et al.*

A

$$P(R,t)= \frac{R}{2Dt} \exp - \frac{R^2}{4Dt}$$

Normal diffusion model

End-tethered Rouse model

— $\Delta t = 0.18$ s, n=4663 steps
— $\Delta t = 1.0$ s, n=3441 steps
— $\Delta t = 1.6$ s, n=2785 steps

B

Figure 5   Hajjoul / Mathon et al.

A

l_p = 200 nm
l_p = 50 nm
l_p = 5 nm

MSD (μm^2)

Δt (s)

B

$$\frac{MSD\,(\tau)}{l_p^2} = \frac{4}{3\pi} \times \left(\frac{\tau k_B T}{\eta l_p^3} \right)^{0.5}$$

MSD / l_p^2

$\tau k_B T / \eta l_p^3$

C

Δt = 0.1 s (n=25)
Δt = 0.6 s (n=73)
Δt = 4.0 s (n=72)

Occurence (%)

Mean Square displacement of
individual trajectories (10^{-3} μm^2)

Figure 6   Hajjoul / Mathon et al.